

## Precision-Spectroscopic Determination of the Binding Energy of a Two-Body Quantum System: The Hydrogen Atom and the Proton-Size Puzzle

Simon Scheidegger<sup>1,2</sup> and Frédéric Merkt<sup>1,2,3,\*</sup>

<sup>1</sup>*Department of Chemistry and Applied Biosciences, ETH Zurich, Zurich 8093, Switzerland*

<sup>2</sup>*Quantum Center, ETH Zurich, Zurich 8093, Switzerland*

<sup>3</sup>*Department of Physics, ETH Zurich, Zurich 8093, Switzerland*

 (Received 27 October 2023; revised 18 January 2024; accepted 25 January 2024; published 11 March 2024)

Precision measurements in Rydberg states of H with principal quantum number  $n$  in the range between 20 and 30 are reported. In the presence of homogeneous electric fields with strengths below  $2 \text{ V cm}^{-1}$ , these Rydberg states are subject to a linear Stark effect with accurately calculable Stark shifts. From the spectral positions of field-independent and field-dependent Rydberg-Stark states, we derive the  $n = 20$  and 24 Bohr energies, and the ionization energy with respect to the  $2^2S_{1/2}(f = 0, 1)$  [short  $2S(0, 1)$ ] metastable states. Combining these results with the  $2S(1) - 1S(1)$  transition frequency [C. G. Parthey *et al.*, *Phys. Rev. Lett.* **107**, 203001 (2011); A. Matveev *et al.*, *Phys. Rev. Lett.* **110**, 230801 (2013)] and the  $1S$  hyperfine splitting [L. Essen *et al.*, *Nature (London)* **229**, 110 (1971)], we determine the ionization frequency of the  $1S(0)$  ground state to be  $3\,288\,087\,922\,407.2(3.7)_{\text{stat}}(1.8)_{\text{syst}}$  kHz, which is the most precise value ever determined for the binding energy of a two-body quantum system. Using the  $2S(0) - 2P_{1/2}(1)$  interval [N. Bezginov *et al.*, *Science* **365**, 1007 (2019)], we determine the Rydberg frequency to be  $cR_\infty = 3\,289\,841\,960\,204(15)_{\text{stat}}(7)_{\text{syst}}(13)_{2S-2P}$  kHz in a procedure that is insensitive to the value of the proton charge radius. These new results are discussed in the context of the proton-size puzzle.

DOI: [10.1103/PhysRevLett.132.113001](https://doi.org/10.1103/PhysRevLett.132.113001)

The H atom is of fundamental importance in quantum physics and metrology. Its two-body properties can be accurately calculated from first principles [1,2]. Precision measurements of transition frequencies in H are used to verify the validity of atomic-structure theory, i.e., relativistic quantum mechanics and quantum electrodynamics, and to determine physical constants such as the Rydberg constant  $R_\infty$  and the proton charge radius  $r_p$ . Until 2010, the values of  $R_\infty$  and  $r_p$ , as reported in the CODATA 2010 global evaluation of physical constants [3], were primarily defined by transition frequencies connecting the  $1S$  and  $2S$  levels to  $nS$ ,  $P$ , and  $D$  levels with principal quantum number  $n$  up to 12 [4–15]. In 2010, these values were challenged by measurements of the  $2S-2P$  intervals in muonic hydrogen ( $\mu\text{H}$ ) [16,17], which yielded an  $r_p$  value  $7\sigma$  below the CODATA 2010 value. Since 2010, new measurements of transition frequencies in H were carried out to shed light on the origin of this discrepancy called the “proton-size puzzle” [18–24]. Although  $R_\infty$  and  $r_p$  were revised in the CODATA 2018 adjustment based on the evaluation of multiple results in H and  $\mu\text{H}$  [2], there are some deviating results and inconsistencies which require clarification.

All transitions reported with high accuracy so far involve the long-lived  $1S$  and/or  $2S$  levels. The energies of these two proton-penetrating states are sensitive to  $r_p$ , which leads to the correlation between  $R_\infty$  and  $r_p$  that is at the

heart of the proton-size puzzle. A possible route to resolve this puzzle consists in measuring transitions involving proton-nonpenetrating high- $n$  Rydberg states of H, which are also long-lived but insensitive to  $r_p$ , and determining  $R_\infty$ . Optical transitions involving high- $n$  levels are affected by their sensitivity to stray fields and have not been considered so far.

Submillimeter-wave transitions between circular  $\ell = n - 1$ ,  $|m_\ell| = \ell$  Rydberg states with  $n \approx 30$  were measured at MIT in a pioneering effort to determine  $R_\infty$  independently of  $r_p$  [25], and new experiments involving circular Rydberg states have recently been proposed to resolve the proton-size puzzle [26,27]. However, their low  $(1/n^3)$  sensitivity to  $R_\infty$  requires extreme frequency accuracy.

We have recently demonstrated that precision measurements on high- $n$  levels at optical frequencies can be performed if they are carried out in well-controlled electric fields [28]. We present here a new measurement of  $R_\infty$  based on optical transitions to proton-nonpenetrating  $n = 20$  and  $n = 24$ ,  $|m_\ell| = 1$  Rydberg-Stark states from which we derive a value of the ionization energy of H of unprecedented accuracy and with which we contribute to resolving the proton-size puzzle.

Figure 1 illustrates our procedure to determine the binding or ionization energy  $E_{\text{bind}} = h\nu_i^{1S(0)}$  of H and the Rydberg constant  $R_\infty$  from measurements of the

transition frequencies  $\nu_1$  (blue arrow) from the  $2S(1)$  state to field-insensitive  $k = 0$  Stark states of principal quantum number  $n = 20$  and  $24$  in the presence of intentionally applied electric fields of strength  $\mathcal{F}$ . The figure depicts the structure of  $n = 1$  and  $n = 2$ ,  $j = 1/2$  states that is accurately known from measurements of the  $2S(1) - 1S(1)$  ( $\nu_4$ ) [15,18], the  $2S$  hyperfine ( $\nu_2$ ) [29], the  $1S$  hyperfine ( $\nu_5$ ) [30], and the  $2S(0) - 2P_{1/2}(1)$  ( $\nu_3$ ) [22] intervals. The ionization energy of the H  $1S(0)$  ground state is given by

$$\nu_i^{1S(0)} = \nu_1 + \nu_4 + \nu_5 + |\delta\nu_{\text{Stark}}^{(n)}(\mathcal{F})| + |\delta\nu_{\text{Stark}}^{(2)}(\mathcal{F})| + c \frac{R_\infty}{n^2} \frac{\mu}{m_e}, \quad (1)$$

where  $\mu$  is the reduced mass  $[(m_e m_p)/(m_e + m_p)]^{-1}$ ,  $\delta\nu_{\text{Stark}}^{(2)}(\mathcal{F})$  are the Stark shifts of the  $2S(f)$  states (see Fig. 6 of Ref. [28]), and  $\delta\nu_{\text{Stark}}^{(n)}(\mathcal{F})$  are the field-dependent shifts of the  $n$ ,  $k = 0$  Rydberg-Stark states from the corresponding Bohr energy. The Rydberg frequency  $cR_\infty$  can be determined using

$$cR_\infty \left[ \left( \frac{1}{4} - \frac{1}{n^2} \right) \frac{\mu}{m_e} + |\delta_{\text{rel,QED}}^{(2)}| \right] = \nu_1 + \nu_2 + \nu_3 + |\delta\nu_{\text{Stark}}^{(n)}(\mathcal{F})| + \delta\nu_{\text{Stark}}^{(2)}(\mathcal{F}), \quad (2)$$

where the first term on the left-hand side is Balmer's formula [31] and  $cR_\infty \delta_{\text{rel,QED}}^{(2)}$  (green bar in Fig. 1)

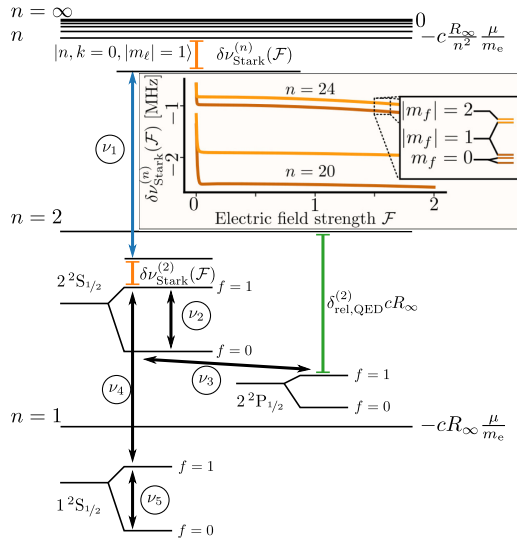


FIG. 1. Energy-level diagram of the  $j = 1/2$  states of the  $n = 1$  and  $2$  manifolds of H and schematic structure of the high- $n$  Rydberg states. The field-dependent energy shift  $\delta\nu_{\text{Stark}}^{(n)}(\mathcal{F})$  of the  $n = 20$  and  $24$ ,  $k = 0$ ,  $|m_\ell| = 1$  Stark states are depicted as orange lines. The field strength is given in V/cm. The inset shows their substructure.

corresponds to the shift of the  $2P_{1/2}(1)$  level from the  $n = 2$  Bohr energy, i.e.,  $-13\,679\,071.1$  kHz [2,32]. Because  $\delta\nu_{\text{Stark}}^{(2)}(\mathcal{F})$ ,  $\delta\nu_{\text{Stark}}^{(n)}(\mathcal{F})$ , and  $\delta_{\text{rel,QED}}^{(2)}$  are accurately calculable (see below) and insensitive to the value of  $r_p$ , a measurement of  $\nu_1$  in combination with Eq. (3) offers a way to determine  $R_\infty$  that is not affected by the correlation between  $r_p$  and  $R_\infty$ .

The experimental setup is depicted schematically in Fig. 2 and is described in Refs. [28,33]. The measurements are carried out at a repetition rate of 25 Hz with a pulsed doubly skimmed supersonic beam of H atoms generated by a cryogenic pulsed valve equipped with a dielectric-barrier discharge. The H-beam characteristics are presented in Ref. [33]. Its narrow transverse-velocity ( $v_x, v_y$ ) distribution corresponds to a temperature of  $40\ \mu\text{K}$ , and the average beam velocity ( $v_z$ ) can be adjusted from 1000 to  $1700\ \text{ms}^{-1}$  by changing the valve temperature between 40 and 160 K.

The Rydberg states of H are accessed in a two-step process in a magnetically shielded photoexcitation region. First, the hyperfine-resolved  $2S-1S$  two-photon transition is induced by the pulse-amplified and frequency-tripled 243-nm output of a cw Ti:sapphire ring laser operated at 729 nm. The long-lived  $2S$  atoms are then excited to

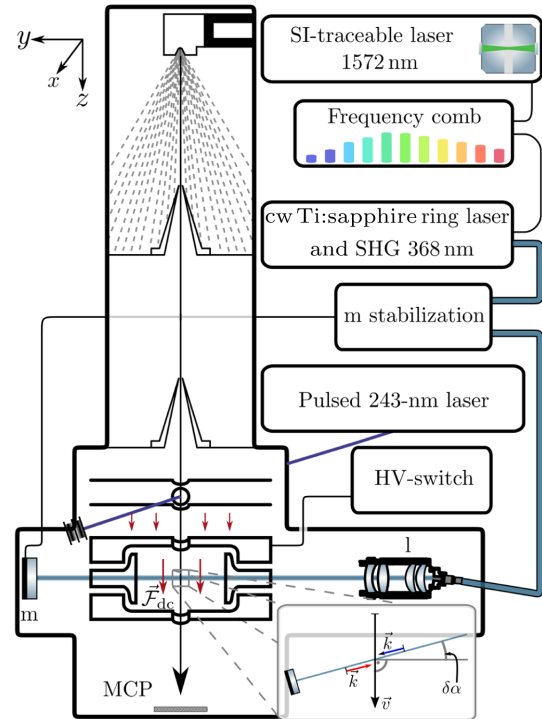


FIG. 2. Schematic representation of the experimental setup with the vacuum chamber comprising the supersonic-beam source and the photoexcitation region (left) and the main components of the laser system (right) (SHG, second harmonic generation; l, lens assembly; m, retroreflecting mirror; MCP, microchannel-plate detector; HV, high-voltage).

Rydberg-Stark states in an intentionally applied homogeneous electric field of strength  $\mathcal{F}$  by a tunable single-mode (bandwidth  $\leq 1$  kHz), linearly polarized ( $x$ ) cw UV laser ( $\lambda = 368$  nm) after traveling a 4-cm-long distance over which ions generated during the  $2S-1S$  excitation are rejected by the applied electric field. The UV laser propagates in a near-orthogonal configuration with respect to the supersonic beam, with an adjustable misalignment angle  $\delta\alpha$  (see bottom right of Fig. 2). The UV laser is introduced into the vacuum chamber through an optical fiber. The divergent beam leaving the fiber is collimated with an aberration-compensating set of four lenses [28]. After traversing the gas sample, the laser is retroreflected by a mirror, giving rise to two Doppler components per line separated by

$$2\nu_D = 2\nu_0 \sin(\delta\alpha)v_z/c. \quad (3)$$

The first-order Doppler-free transition frequencies ( $\nu_0$ ) are obtained by averaging the frequencies of the two Doppler components. The stabilization of the retroreflection arrangement is inspired by Refs. [34,35] and involves the active control of the mirror angles using two actuators (one for each mirror axis) to optimize the intensity of the reflected beam after recoupling it into the fiber out of which the forward-propagating beam emerged. The full width at half maximum of the angular acceptance of the recoupling of the reflected beam is  $67(5)$   $\mu\text{rad}$ . By dithering the mirror angles and using lock-in amplifiers, dispersion signals are generated and used to stabilize the retroreflection angle at  $180^\circ$ .

Rydberg-excitation spectra are recorded by monitoring the protons generated by pulsed field ionization as a function of the UV laser frequency using a microchannel-plate (MCP) detector. The strength of the pulsed field is chosen to be large enough to completely ionize the Rydberg-atom sample. This measure guarantees a  $4\pi$ -field-of-view detection, which is crucial to avoid systematic errors from quantum interference [36]. The cw-laser frequency is referenced to an SI-traceable optical frequency distributed through a phase-stabilized network [37]. The electric field strength  $\mathcal{F}$  ( $\vec{\mathcal{F}} = \mathcal{F}_z\vec{e}_z + \vec{\mathcal{F}}_{\text{stray}}$ ) in the photoexcitation region is determined with an accuracy of  $500 \mu\text{V cm}^{-1}$  by measuring the spectral separation between the field-sensitive  $k = \pm 2$  Stark states (see Fig. 3 and Ref. [28]).

We use Eq. (3) to relate the frequencies of the  $n, k, |m_\ell| = 1 \leftarrow 2S(f)$  transitions measured in the presence of an intentionally applied electric field of strength  $\mathcal{F}$  to the Rydberg constant  $R_\infty$ . To calculate  $\delta\nu_{\text{Stark}}^{(2)}(\mathcal{F})$  and  $\delta\nu_{\text{Stark}}^{(n)}(\mathcal{F})$ , we evaluate the effect of the Stark operator  $e\mathcal{F}\hat{z}$  on the level structure, as described in Ref. [28]. In brief, we set up the Hamiltonian matrix

$$\hat{\mathcal{H}} = \hat{\mathcal{H}}_0 + e\mathcal{F}\hat{z}, \quad (4)$$

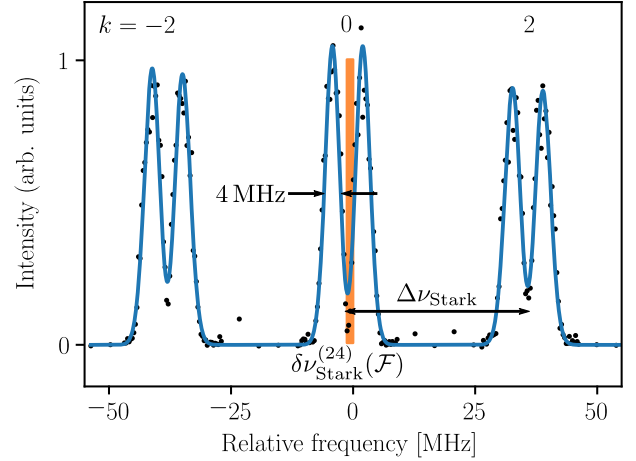


FIG. 3. Spectrum of the transitions from the  $2S(1)$  state of H to the  $n = 24, k = \pm 2, 0, |m_\ell| = 1$  Stark states (black dots) and spectrum calculated with the line-shape parameters obtained from a weighted least-squares fit (blue line). The width of the orange area corresponds to  $\delta\nu_{\text{Stark}}^{(24)}(0.4 \text{ V cm}^{-1})$ , which bridges the observed transition frequency to the Bohr energy at 0 MHz.

in the spherical basis, where  $\hat{\mathcal{H}}_0$  is a diagonal matrix with eigenvalues calculated considering relativistic, QED, and finite-nuclear-size effects using Eqs. (7)–(41) of Ref. [2] and the hyperfine splittings reported in Ref. [32]. The eigenvalues of  $\hat{\mathcal{H}}_0$  for the  $n = 2, 20$ , and  $24$  Rydberg states relevant for the present investigation are tabulated in the Supplemental Material [38]. The eigenvalues of  $\hat{\mathcal{H}}$  represent the field-dependent level energies, with Stark shifts displayed in Fig. 1 for  $n = 20$  ( $24$ )  $k = 0, |m_\ell| = 1, |m_f| = 1$ . Numerical values for the Stark shifts at  $\mathcal{F} = 0.4$  and  $0.8 \text{ V cm}^{-1}$  of all  $k = 0$  Stark states relevant for the present study are also listed in the Supplemental Material [38]. These Stark shifts are so small that they are not sensitive to the exact value of  $R_\infty$ .

525 spectra of transitions from the  $2S(0, 1)$  to  $n, k = 0, \pm 2, |m_\ell| = 1$  Stark states with  $n = 20$  and  $24$  were recorded at beam velocities between  $1000$  and  $1700 \text{ ms}^{-1}$ , misalignment angles  $\delta\alpha$  in the range between  $0.1$  and  $0.06^\circ$ , and electric field strengths  $\mathcal{F}$  between  $0.4$  and  $1.6 \text{ V cm}^{-1}$ . Figure 3 shows, as example, a spectrum of the  $n = 24, k = 0, \pm 2, |m_\ell| = 1 \leftarrow 2S(1)$  transition (black dots) and the spectrum calculated after fitting the line shape with Eqs. (4) and (5) of Ref. [28]. The results of all measurements, including a discussion of the main uncertainties, are presented in Appendix A, and the error budget is summarized in Table I.

The transition frequencies are corrected by the photon-recoil shifts of  $-1458.8$  and  $-1467.8 \text{ kHz}$  for transitions to  $n = 20$  and  $n = 24$ , respectively. The correction for the second-order-Doppler shift  $\delta\nu_{D(2)} = \frac{1}{2}(v/c)v_1$  is calculated from the H-atom beam velocities  $v$ . The beam velocities are measured within an uncertainty of  $12 \text{ ms}^{-1}$  [33], resulting in a systematic uncertainty of  $120 \text{ Hz}$ .

TABLE I. Corrections and uncertainties considered in the determination of the ionization frequency of H[2S(1)]. All values and uncertainties are reported in kHz. See text for details.

	$\Delta\nu$	$\sigma_{\text{stat}}$	$\sigma_{\text{syst}}$
First-order Doppler shift $\delta\nu_{D(1)}$	0	2.4	0
Second-order Doppler shift $\delta\nu_{D(2)}$	4.5	0	0.12
Residual quadratic Stark shift $\delta\nu_{\mathcal{F}^2}$	0	1.6	0
ac-Stark shift (TR) $\delta\nu_{\text{ac-Stark}}^{(\text{TR})}$	-2.2	0	1.1
Zeeman shift	0	0	0.56
Pressure shift	0	0	0.05
Photon recoil shift ( $n = 20$ )	-1458.8	0	0
Photon recoil shift ( $n = 24$ )	-1467.8	0	0

The ac-Stark shift induced by 298 K thermal radiation (TR)  $\delta\nu_{\text{ac-Stark}}^{(\text{TR})}$  is -2.2 kHz [39]. Because the thermal radiation in the photoexcitation region may slightly deviate from that of a pure 298 K blackbody emitter, we assume a systematic uncertainty of  $\pm 1.1$  kHz on  $\delta\nu_{\text{ac-Stark}}^{(\text{TR})}$ .

The orthogonal configuration between the cw-laser propagation direction ( $y$ ) and the quantization axis ( $z$ ) given by the applied electric field prevents optical pumping between Zeeman sublevels in the residual magnetic field ( $< 1$  mG). Consequently, Zeeman shifts can only occur from an unbalanced  $m_f$  population in the 2S(1) state, which causes a systematic uncertainty of the order of  $g_L\mu_B|B_{\text{res}}|/5 = 560$  Hz.

The pressure shifts of Rydberg states caused by H<sub>2</sub> are characterized by a coefficient of 5.4 kHz/(10<sup>12</sup>/cm<sup>3</sup>) [40,41]. The density of H<sub>2</sub> molecules in the photoexcitation volume is less than 10<sup>10</sup>/cm<sup>3</sup> [33] and results in an systematic uncertainty of 50 Hz.

Systematic errors from quantum-interference effects [36] are negligible in the present experiments because of the 4 $\pi$ -field-of-view detection. Possible line shifts resulting from momentum transfer from repeated absorption-emission cycles are negligible because the natural linewidth  $\Gamma$  ( $\approx 8$  kHz) is much narrower than the recoil shift ( $\nu_{\text{recoil}}/\Gamma \approx 180$ ), which rules out more than one absorption event. Finally, line shifts from dipole-dipole interactions between Rydberg atoms are also negligible because only one H atom is excited to a Rydberg state in  $\sim 3$  experimental cycles.

The absolute transition frequencies to the  $n = 20$  and 24 Bohr levels are determined to be  $\nu[20 \leftarrow 2S(0)] = 813\,805\,449\,014.0(7.4)_{\text{stat}}(1.8)_{\text{syst}}$  kHz,  $\nu[20 \leftarrow 2S(1)] = 813\,805\,271\,445.1(4.5)_{\text{stat}}(1.8)_{\text{syst}}$  kHz,  $\nu[24 \leftarrow 2S(1)] = 816\,316\,977\,250.3(4.6)_{\text{stat}}(1.8)_{\text{syst}}$  kHz. The final result for the H<sup>+</sup> + e<sup>-</sup>  $\leftarrow$  H[2S(1)] ionization frequency is

$$\nu_i^{2S(1)} = 822\,025\,399\,526.6(3.7)_{\text{stat}}(1.8)_{\text{syst}} \text{ kHz.}$$

This value can be combined with the accurately known 2S(1)–1S(1) transition frequency [15,18] and the 1S hyperfine interval [30] to obtain

$$\nu_i^{1S(0)} = 3\,288\,087\,922\,407.2(3.7)_{\text{stat}}(1.8)_{\text{syst}} \text{ kHz}$$

for the ionization frequency of the 1S(0) ground state of the H atom. The 2S(1)–1S(1) and the 1S hyperfine intervals are so accurately known [15,18,30] that the uncertainty in  $\nu_i^{1S(0)}$  is entirely given by the 2S(1) ionization frequency determined in the present work.  $\nu_i^{1S(0)}$  represents the most precise experimental value for the binding energy of a two-body quantum system reported so far. This result is in agreement with, but more precise than, the value of 3 288 087 922 416.2(6.4)<sub>R $\infty$</sub> (1.6)<sub>calc</sub> kHz one can calculate using Eqs. (7)–(41) of Ref. [2] and the 1S hyperfine interval from Ref. [30]. In principle,  $\nu_i^{1S(0)}$  could also be determined from the measurements of other intervals such as the 2S–4P [20] and 2S–8D [24] intervals following a similar procedure to that used here.

The Rydberg frequency obtained with Eq. (3) is

$$cR_\infty = 3\,289\,841\,960\,204(15)_{\text{stat}}(7)_{\text{syst}}(13)_{2S-2P} \text{ kHz.}$$

Because the interval from which  $R_\infty$  is determined is approximately  $R_\infty/4$ , the uncertainties increase by a factor of 4. The uncertainty  $\sigma_{2S-2P}$  of  $4 \times 3.2$  kHz arises from the 3.2 kHz uncertainty of the 2S(0)–2P(1) frequency reported by Bezginov *et al.* [22]. The procedure used here to determine  $R_\infty$  by combining transitions measured from the 2S level with the measurement of Ref. [22] can also be applied to the 2S–8D interval from Ref. [24] and the 2S–4S intervals from Ref. [20]. The resulting values are listed in Table II in Appendix B.

Figure 4 compares the  $R_\infty$  value obtained in this work (horizontal turquoise line) with values determined from millimeter-wave spectroscopy of transitions between  $n = 27$ –30 circular Rydberg states in the group of D. Kleppner at MIT [25], the  $cR_\infty$  values recommended in the 2010 fundamental-constant adjustment [3], and the  $cR_\infty$  value obtained in the latest CODATA evaluation [2], which includes the Lamb-shift measurement in muonic hydrogen [16,17], and the individual measurements of frequency intervals in H reported since 2010 [20–24]. Whereas the  $cR_\infty$  value reported by De Vries [25] is compatible with both CODATA values, the result for  $cR_\infty$  presented here lies 1.3 $\sigma$  below the CODATA 2018 value and 4.5 $\sigma$  below the CODATA 2010 value. Combining our measurement with the  $r_p$  value from Refs. [16,17] gives a  $cR_\infty$  value of 3 289 841 960 214(22) kHz (see turquoise diamond in Fig. 4). The uncertainty  $\sigma_{2S-2P}$  does not contribute in this case. In combination with the 1S–2S transition frequency from Refs. [15,18], our measurement yields a  $cR_\infty$  value of 3 289 841 960 194(40) kHz and an  $r_p$  value of 0.822(13) fm

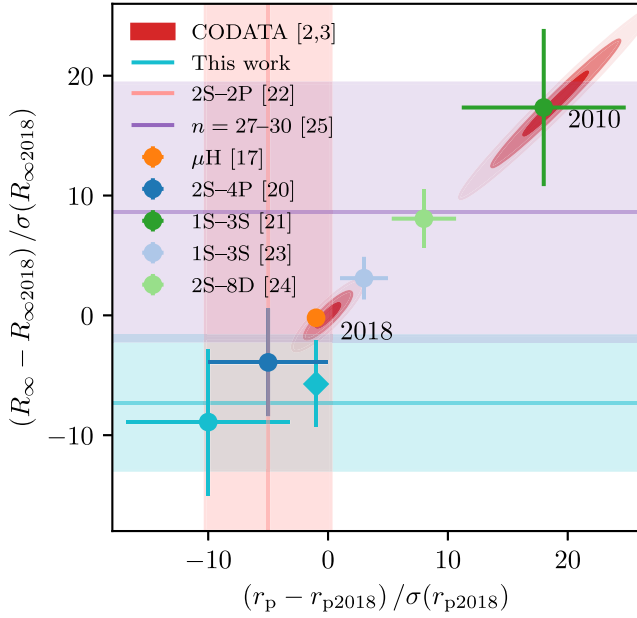


FIG. 4. Scatter plot of  $(R_\infty, r_p)$  values from transition frequencies in H [20–24] since 2010 relative to the values reported in Tiesinga *et al.* [2], in units of the CODATA 2018 uncertainties. The covariance ellipses with the  $1\sigma$ ,  $2\sigma$ , and  $3\sigma$  intervals of the CODATA 2018 and 2010 adjustments [2,3] are in red. When only  $R_\infty$  or  $r_p$  are reported the data are represented as vertical or horizontal lines with uncertainties given by shaded areas for  $r_p$  or  $R_\infty$ , respectively.

(turquoise dot with double error bars) following the procedure described in Ref. [2].

The  $2S-2P_{3/2}$  transitions in muonic hydrogen ( $\mu\text{H}$ ) [16] are almost exclusively sensitive to the proton rms charge radius  $r_p$  and not to  $R_\infty$ , whereas the measurement presented here, when combined with the measurement of Ref. [22], is almost exclusively sensitive to  $R_\infty$  and not to  $r_p$ . The two determinations are thus independent of the correlation between  $R_\infty$  and  $r_p$  which affects most

determinations of these quantities based on transitions of the H atom. The significance of the present results, next to the unprecedented precision of  $\nu_i^{1S(0)}$ , is that they were obtained from spectra of the H atom and indirectly confirm the  $r_p$  value obtained in the  $\mu\text{H}$  experiments [16,17] through the  $R_\infty$  value. Consequently, the discrepancies in Fig. 4 cannot be attributed to beyond-the-standard-model differences in the physical laws governing the properties of H and  $\mu\text{H}$ . This consideration is already implemented in the CODATA 2018 revision, which had, however, to increase the error bars because of existing deviating experiments [2]. In our opinion, one could go one step further and use the  $(R_\infty, r_p)$  values given by the orange dot in Fig. 4 and obtained by combining the results of the measurements of the  $2S-1S$  transition in H [15,18] and the Lamb-shift in  $\mu\text{H}$  [16,17].

This work was supported by the Swiss National Science Foundation through a Sinergia-program grant (No. CRSII5-183579) and a single-investigator grant (No. 200020B-200478). We thank H. Schmutz, J. A. Agner, P. Jansen, and G. Clausen for experimental help and discussions, and J. Morel and D. Husmann (both at METAS), J. Faist (ETH Zurich), S. Willitsch (University of Basel), and E. Heiri and F. Mauchle (Switch Foundation) for their contributions to setting up the SI-traceable frequency-distribution system used in this work.

*Appendix A: On the measured transition frequencies and their uncertainties.*—Figure 5(a) presents the corresponding ionization frequencies  $\nu_i^{2S(1)}$  obtained from the  $n = 20-2S(0)$  (blue),  $n = 20-2S(1)$  (orange), and  $n = 24-2S(1)$  (green) transitions. The thick black horizontal line represents the mean of all ionization energies and the dotted lines give the standard deviation. The standard deviations of the mean from the three color-coded subsets and the total dataset are depicted on an enlarged scale on the right. The black error bars

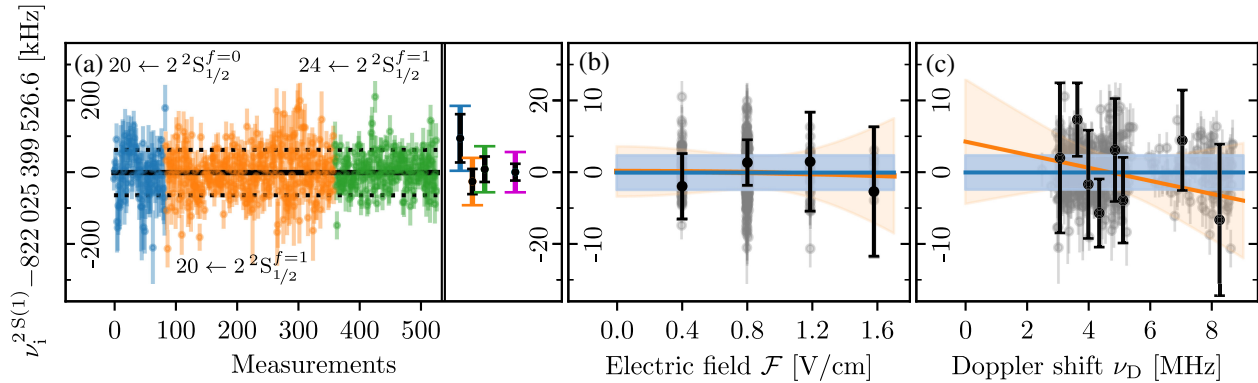


FIG. 5. (a) Ionization frequencies  $\nu_i^{2S(1)}$  obtained from the frequencies  $\nu(20 \leftarrow 2^2S_{1/2}^{f=0})$  (blue),  $\nu(20 \leftarrow 2^2S_{1/2}^{f=1})$  (orange), and  $\nu(24 \leftarrow 2^2S_{1/2}^{f=1})$  (green). (b),(c) Dependence of the ionization frequency on the electric field strength  $\mathcal{F}$  (b) and on the Doppler shift  $\nu_D$  (c) (see text for details).

correspond to the dispersion of the experimental results with statistical uncertainties of 6.8, 3.5, and 3.6 kHz of the individual datasets, and 2.4 kHz for the combined dataset. The error bars in color (magenta for the full dataset) are the total uncertainties including the systematic uncertainties, which are defined in Table I above.

The two main potential sources of systematic uncertainties are (i) residual quadratic Stark shifts from electric field inhomogeneities in the photoexcitation volume, which we model with a quadratic function,

$$\nu_i(\mathcal{F}) = \nu_i(0) + b\mathcal{F}^2, \quad (\text{A1})$$

and (ii) residual first-order Doppler shifts from an imperfect alignment of the reflection mirror, which are proportional to the Doppler shift  $\nu_D$ ,

$$\nu_i(\nu_D) = \nu_i(0) + a\nu_D. \quad (\text{A2})$$

Figures 5(b) and 5(c) depict the dependence of the ionization frequency  $\nu_i^{2S(1)}$  on the applied electric field  $\mathcal{F}$  [Fig. 5(b)] and on the Doppler shift  $\nu_D$  [Fig. 5(c)]. The gray dots (ordinate scaled by 1:20) are individual measurements, the black dots are sample averages, and the uncertainties are indicated by the error bars. The blue and orange lines indicate, respectively, the mean ionization frequency and the extrapolations with Eqs. (A1) or (A2). The corresponding  $1\sigma$  confidence intervals are depicted as blue and orange shaded areas. From least-squares fits of the full dataset, we obtain  $b = -0.3(3.5) \text{ kHz}(\text{V cm}^{-1})^{-2}$  and  $a = -0.9(1.8) \text{ kHz}(\text{MHz})^{-1}$ . Because both parameters are compatible with zero, we do not correct the ionization frequency but include the corresponding uncertainties.

The statistical uncertainty of the first-order Doppler shift  $\sigma_{\delta\nu_{p(1)}} = \langle \nu_D \rangle \sigma_a = 2.4 \text{ kHz}$  is obtained by multiplying the sample mean of the observed Doppler shift  $\langle \nu_D \rangle = 4.8 \text{ MHz}$  with the standard error  $\sigma_a = 0.5 \text{ kHz}(\text{MHz})^{-1}$  of the slope  $a$  of the residual Doppler shift obtained in a least-squares fit of the expression  $\nu_i(\nu_D) = \langle \nu_i \rangle + a\nu_D$  to the data. In an analogous procedure, we estimate the statistical uncertainty of a potential residual quadratic Stark shift to be  $\sigma_{\delta\nu_{\mathcal{F}^2}} = \langle \mathcal{F}^2 \rangle \sigma_b = 1.6 \text{ kHz}$  using the expression  $\nu_i(\mathcal{F}) = \langle \nu_i \rangle + b\mathcal{F}^2$ .

*Appendix B: On the comparison of  $R_\infty$  values determined using  $r_p$ -insensitive procedures with CODATA values.*—Table II compares the Rydberg frequencies  $cR_\infty$  reported in the CODATA 2010 [3] and CODATA 2018 [2] evaluations with the  $cR_\infty$  values determined in an  $r_p$ -independent manner from (i) transitions between circular Rydberg states with  $n$  values around 30 [25], (ii) the combination of the  $2S-4P$  transition frequency [20] with the  $2S(0) - 2P_{1/2}(1)$  transition frequency [22], (iii) the combination

TABLE II. Comparison of  $cR_\infty$  values determined using  $r_p$ -insensitive procedures with CODATA values. All values in kHz.

Transitions	$R_\infty$	Reference
$29c-30c$	3 289 841 960 306(69)	[25]
$2S-4P$ , $2S-2P$	3 289 841 960 226(29)	[20,22]
$2S-8D$ , $2S-2P$	3 289 841 960 268(22)	[22,24]
$2S$ -high $n$	3 289 841 960 204(35)	This work, [22]
CODATA 2010	3 289 841 960 365(16)	[3]
CODATA 2018	3 289 841 960 250.8(6.4)	[2]

of the  $2S-8D$  transition frequency [24] with the  $2S(0) - 2P_{1/2}(1)$  transition frequency [22], and the combination of the  $2S$ -high  $n$  transitions frequencies from this work with the  $2S(0) - 2P_{1/2}(1)$  transition frequency.

\*merkt@phys.chem.ethz.ch

- [1] V. A. Yerokhin, K. Pachucki, and V. Patkóš, *Ann. Phys. (Amsterdam)* **531**, 1800324 (2019).
- [2] E. Tiesinga, P. J. Mohr, D. B. Newell, and B. N. Taylor, *Rev. Mod. Phys.* **93**, 025010 (2021).
- [3] P. J. Mohr, B. N. Taylor, and D. B. Newell, *Rev. Mod. Phys.* **84**, 1527 (2012).
- [4] G. Newton, D. A. Andrews, and P. J. Unsworth, *Phil. Trans. R. Soc. A* **290**, 373 (1979).
- [5] S. R. Lundeen and F. M. Pipkin, *Metrologia* **22**, 9 (1986).
- [6] E. W. Hagley and F. M. Pipkin, *Phys. Rev. Lett.* **72**, 1172 (1994).
- [7] M. Weitz, A. Huber, F. Schmidt-Kaler, D. Leibfried, W. Vassen, C. Zimmermann, K. Pachucki, T. W. Hänsch, L. Julien, and F. Biraben, *Phys. Rev. A* **52**, 2664 (1995).
- [8] D. J. Berkeland, E. A. Hinds, and M. G. Boshier, *Phys. Rev. Lett.* **75**, 2470 (1995).
- [9] S. Bourzeix, B. de Beauvoir, F. Nez, M. D. Plimmer, F. de Tomasi, L. Julien, F. Biraben, and D. N. Stacey, *Phys. Rev. Lett.* **76**, 384 (1996).
- [10] B. de Beauvoir, F. Nez, L. Julien, B. Cagnac, F. Biraben, D. Touahri, L. Hilico, O. Acef, A. Clairon, and J. J. Zondy, *Phys. Rev. Lett.* **78**, 440 (1997).
- [11] C. Schwob, L. Jozefowski, B. de Beauvoir, L. Hilico, F. Nez, L. Julien, F. Biraben, O. Acef, J.-J. Zondy, and A. Clairon, *Phys. Rev. Lett.* **82**, 4960 (1999).
- [12] M. Fischer, N. Kolachevsky, M. Zimmermann, R. Holzwarth, Th. Udem, T. W. Hänsch, M. Abgrall, J. Grünert, I. Maksimovic, S. Bize, H. Marion, F. P. Dos Santos, P. Lemonde, G. Santarelli, P. Laurent, A. Clairon, C. Salomon, M. Haas, U. D. Jentschura, and C. H. Keitel, *Phys. Rev. Lett.* **92**, 230802 (2004).
- [13] O. Arnoult, F. Nez, L. Julien, and F. Biraben, *Eur. Phys. J. D* **60**, 243 (2010).
- [14] C. G. Parthey, A. Matveev, J. Alnis, R. Pohl, T. Udem, U. D. Jentschura, N. Kolachevsky, and T. W. Hänsch, *Phys. Rev. Lett.* **104**, 233001 (2010).
- [15] C. G. Parthey, A. Matveev, J. Alnis, B. Bernhardt, A. Beyer, R. Holzwarth, A. Maistrou, R. Pohl, K. Predehl, T. Udem, T. Wilken, N. Kolachevsky, M. Abgrall, D. Rovera,

- C. Salomon, P. Laurent, and T. W. Hänsch, *Phys. Rev. Lett.* **107**, 203001 (2011).
- [16] R. Pohl *et al.*, *Nature (London)* **466**, 213 (2010).
- [17] A. Antognini *et al.*, *Science* **339**, 417 (2013).
- [18] A. Matveev, C. G. Parthey, K. Predehl, J. Alnis, A. Beyer, R. Holzwarth, T. Udem, T. Wilken, N. Kolachevsky, M. Abgrall, D. Rovera, C. Salomon, P. Laurent, G. Grosche, O. Terra, T. Legero, H. Schnatz, S. Weyers, B. Altschul, and T. W. Hänsch, *Phys. Rev. Lett.* **110**, 230801 (2013).
- [19] D. C. Yost, A. Matveev, A. Grinin, E. Peters, L. Maisenbacher, A. Beyer, R. Pohl, N. Kolachevsky, K. Khabarova, T. W. Hänsch, and T. Udem, *Phys. Rev. A* **93**, 042509 (2016).
- [20] A. Beyer, L. Maisenbacher, A. Matveev, R. Pohl, K. Khabarova, A. Grinin, T. Lamour, D. C. Yost, T. W. Hänsch, N. Kolachevsky, and T. Udem, *Science* **358**, 79 (2017).
- [21] H. Fleurbaey, S. Galtier, S. Thomas, M. Bonnaud, L. Julien, F. Biraben, F. Nez, M. Abgrall, and J. Guéna, *Phys. Rev. Lett.* **120**, 183001 (2018).
- [22] N. Bezginov, T. Valdez, M. Horbatsch, A. Marsman, A. C. Vutha, and E. A. Hessels, *Science* **365**, 1007 (2019).
- [23] A. Grinin, A. Matveev, D. C. Yost, L. Maisenbacher, V. Wirthl, R. Pohl, T. W. Hänsch, and T. Udem, *Science* **370**, 1061 (2020).
- [24] A. D. Brandt, S. F. Cooper, C. Rasor, Z. Burkley, A. Matveev, and D. C. Yost, *Phys. Rev. Lett.* **128**, 023001 (2022).
- [25] J. C. De Vries, A precision millimeter-wave measurement of the Rydberg frequency, Ph.D. thesis, MIT, 2002.
- [26] A. Ramos, K. Moore, and G. Raithel, *Phys. Rev. A* **96**, 032513 (2017).
- [27] U. D. Jentschura and D. C. Yost, *Phys. Rev. A* **108**, 062822 (2023).
- [28] S. Scheidegger, J. A. Agner, H. Schmutz, and F. Merkt, *Phys. Rev. A* **108**, 042803 (2023).
- [29] R. G. Bullis, C. Rasor, W. L. Tavis, S. A. Johnson, M. R. Weiss, and D. C. Yost, *Phys. Rev. Lett.* **130**, 203001 (2023).
- [30] L. Essen, R. W. Donaldson, M. J. Bangham, and E. G. Hope, *Nature (London)* **229**, 110 (1971).
- [31] J. J. Balmer, *Ann. Phys. Chem.* **261**, 80 (1885).
- [32] M. Horbatsch and E. A. Hessels, *Phys. Rev. A* **93**, 022513 (2016).
- [33] S. Scheidegger, D. Schlander, J. A. Agner, H. Schmutz, P. Jansen, and F. Merkt, *J. Phys. B* **55**, 155002 (2022).
- [34] A. Beyer, L. Maisenbacher, A. Matveev, R. Pohl, K. Khabarova, Y. Chang, A. Grinin, T. Lamour, T. Shi, D. C. Yost, Th. Udem, T. W. Hänsch, and N. Kolachevsky, *Opt. Express* **24**, 17470 (2016).
- [35] V. Wirthl, L. Maisenbacher, J. Weitenberg, A. Hertlein, A. Grinin, A. Matveev, R. Pohl, T. W. Hänsch, and T. Udem, *Opt. Express* **29**, 7024 (2021).
- [36] T. Udem, L. Maisenbacher, A. Matveev, V. Andreev, A. Grinin, A. Beyer, N. Kolachevsky, R. Pohl, D. C. Yost, and T. W. Hänsch, *Ann. Phys. (Amsterdam)* **531**, 1900044 (2019).
- [37] D. Husmann, L.-G. Bernier, M. Bertrand, D. Calonico, K. Chaloulos, G. Clausen, C. Clivati, J. Faist, E. Heiri, U. Hollenstein, A. Johnson, F. Mauchle, Z. Meir, F. Merkt, A. Mura, G. Scalari, S. Scheidegger, H. Schmutz, M. Sinhal, S. Willitsch, and J. Morel, *Opt. Express* **29**, 24592 (2021).
- [38] See Supplemental Material at <http://link.aps.org/supplemental/10.1103/PhysRevLett.132.113001> for the calculated differences between the  $n = 2, 20$  and  $24$   $ljf$  energies  $E_{nljf}$  of the H atom and the corresponding Bohr energies  $E_n = (2n^2)^{-1}$  and the calculated Stark shifts of the  $k = 0$  Stark states at  $n = 2, 20$  and  $24$  and electric fields of  $0.4$  and  $0.8$  V cm $^{-1}$ .
- [39] J. W. Farley and W. H. Wing, *Phys. Rev. A* **23**, 2397 (1981).
- [40] E. Amaldi and E. Segrè, *Nuovo Cimento* **11**, 145 (1934).
- [41] G. Herzberg and Ch. Jungen, *J. Mol. Spectrosc.* **41**, 425 (1972).